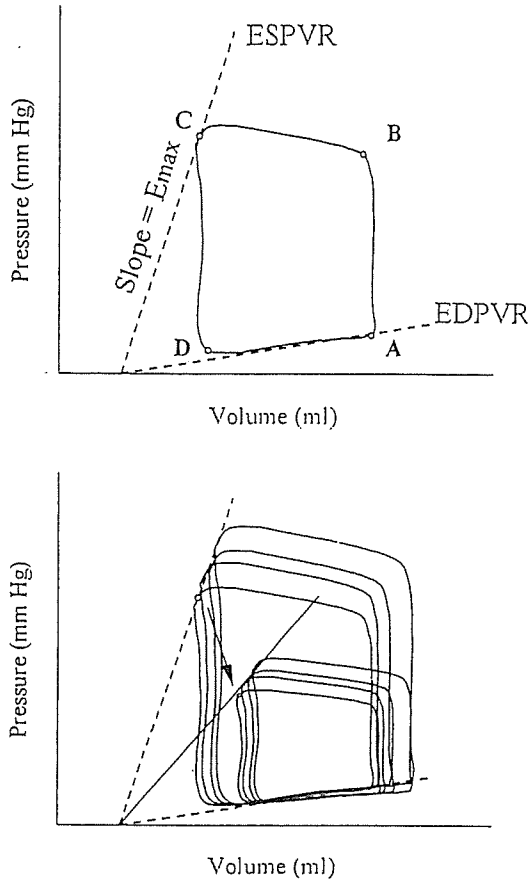

Fig. 2 Upper diagram presents a pressure-volume relationship for a left ventricle in a rat during a single cardiac cycle. From end-diastole (A) pressure increases while volume remains stable (isovolumic) until *B*, when volume rapidly decreases during ejection, but pressure remains high until end-systole (C), then pressure rapidly decreases during relaxation until *D*, when ventricular filling commences. Lower diagram illustrates P-V relations over several consecutive cycles and the change in E_{max} from control conditions (*dashed line*) after the administration of a negative ionotropic agent (*solid line*).

past led to some controversy about its definition and the characteristics of the relation (see Kass and Maughan[33]). Nevertheless, whether ESPVR is considered to be linear or curvilinear it remains as a useful concept to compare left ventricle function under different loading conditions[26]. Many studies have demonstrated that E_{max} changes with ionotropic state and decreases in failing hearts (Fig. 2, lower diagram). E_{max} can be considered to represent the degree of crossbridge attachment at the end of systole.

Total mechanical energy generated during a ventricular contraction was calculated by Suga[25] using the theory of elasticity from the P-V loop area (PVA), which is the area of the figure bounded by the end-systolic and end-diastolic pressure-volume curves and the systolic limb of the pressure-volume curve (Fig. 3). Total mechanical energy is therefore the sum of the potential energy created by the elastance of the ventricle during systole and the external mechanical stroke work. All reports to date have found that PVA (units of mm Hg·ml·beat^{-1}) is highly linearly correlated with cardiac oxygen consumption[25-38]. Contractile efficiency of the left ventricle reflects both the heart's efficiency at generating ATP and the efficiency of crossbridge cycling to convert ATP into mechanical energy. In cross-circulated and isolated canine hearts the contractile efficiency is about 40%, including energy required for the maintenance of the myocardium between contractions, and the remainder is dissipated as heat[25,39]. The amount of energy used for external work, i.e. mechanical efficiency, is 15-30% in hearts with typical ejection fractions of 50%[30]. Already there are indications that the composition of myosin isomers in filaments affects ventricular performance, as well as efficiency. Fast V1 (both α-myosin heavy chains) fibers are less economical than V3 (both β-myosin heavy chains) fibers, but the former can shorten faster and generate greater mechanical power[19,39,40]. Weisberg and Winegrad[41] have also shown that isolated α- and β-myosin heavy chains form crossbridges that differ in structure and flexibility, and furthermore, differ with regard to changes in flexibility during myosin ATPase activity correlating well with their rates of crossbridge cycling. The effects of altered contractile state on ventricular P-V relations and energetics of cardiac contractions have not been examined in transgenic mouse models.

Sunagawa and associates[42] expanded the possibilities of PVA analysis further with an index of effective arterial elastance (E_a), which is the ratio of end-systolic pressure to stroke volume (Fig. 3). The E_a/E_{max} ratio is considered to be a good indication of cardiac efficiency and load matching. Improved accuracy led to *in situ* instantaneous left ventricular volume determinations on a beat-to-

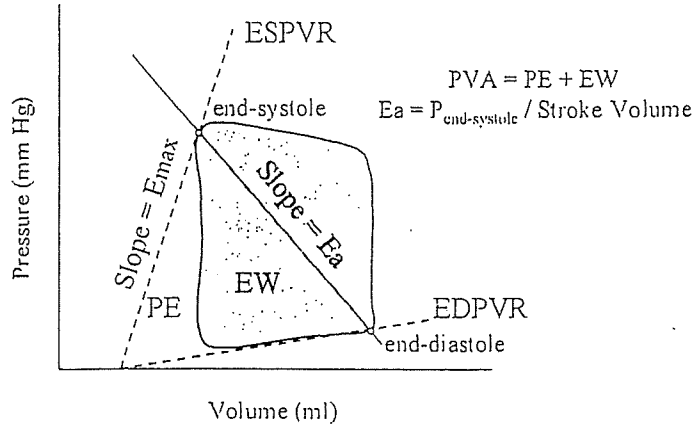

Fig. 3 Pressure-volume area (PVA) is equivalent to the mechanical energy of a contraction and can be partitioned between the elastic potential energy (PE) of the ventricular wall during systole and external work (EW) performed during contraction (see review by Suga[50]). The difference between end-systole and end-diastole P-V points is the stroke volume. Effective arterial elastance (E_a) of the ventricle can be obtained from the slope of the line connecting the end-diastolic volume and ESPV.

beat basis routinely by introducing a conductance catheter directly into the left ventricle from the apex of the heart[35,43–45], or alternatively via atrial and left carotid arterial cannulation[46]. Nevertheless, today we are able to measure both pressure and volume simultaneously in anaesthetized mice[47,48]. The only disadvantage of these current procedures is the need for open-chest surgery, which is particularly difficult and is therefore likely to limit widespread use among researchers until an alternate approach is developed. Further, the loss of intrathoracic pressure negatively influences cardiac and ventilatory performance. Combining X-ray diffraction techniques with P-V loop measurements, *in situ* and in real time, is a physical challenge in itself. Direct exposure of the radiation on the sensor tip of pressure micromanometers might destroy it.

Finally, one more potential problem to be considered relates to experimental protocol. Recently it has been shown that some transgenic models exhibit extensive ventricular arrythmias. Therefore obtaining P-V relations from *in vivo* hearts performing in a stable contractile state may be difficult in such circumstances unless analyses are performed on a beat-to-beat basis, which is now possible at facilities such as SPring-8 (Harima) with fast CCD cameras and a strong synchrotron source.

3. Future Applications of X-ray Diffraction to Gene Therapy-modified Animals

Perhaps the area that we envision the most progress being made with simultaneous measurements of cardiac micro-macro functions is with transgenic mice models, because mice can most easily be used to knockout and over express gene function. With the development of X-ray diffraction and P-V loop measurements *in vivo* mouse hearts, in real time, we will be able to quantify the contribution of individual genes to the overall performance of the heart. Inheritable cardiovascular diseases can be investigated by introducing human DNA into the genome of mice and determining the consequent effects on heart performance. Similarly, the effectiveness of treatment of heart disease using gene therapy to replace genes that confer inadequate function can be explored. Examples of such therapeutic manipulations include replacing sluggish ATPase isozymes that limit membrane excitation and contraction pathways. The rate of myosin ATPase hydrolysis limits the detachment rate of crossbridge from actin, which limits the maximal velocity of shortening of myocardial fibers and is thought to be responsible for the faster velocity of shortening in fast V1 myosin isozymes in comparison to V2

isozymes[49]. Promotion of changes in enzyme composition can therefore greatly alter the performance of the whole heart, which is ultimately the goal of clinical research.

This work was supported in part by the Promotion of Fundamental Studies in Health Sciences of the Organization for Pharmaceutical Safety and Research (OPSR) of Japan; Health Sciences Grant (Funds for Human Genome Research and Regeneration Medicine Research); Grants-in-Aid for Scientific Research (13470154, 13877114) from the Ministry of Education, Culture, Sports, Science and Technology; New Energy and Industrial Technology Development Organization; and The Research Grants for Cardiovascular Disease (H13C-1) from the Ministry of Health, Labor and Welfare.

Bibliography

1) Huxley HE: X-ray analysis and the problem of muscle. Proc R Soc B **141**: 59-62, 1953
2) Matsubara I, Elliott GF: X-ray diffraction studies on skinned single fibres of frog skeletal muscle. J Mol Biol **72**: 657-669, 1972
3) Matsubara I: X-ray diffraction studies of the heart. Annu Rev Biophys Bioeng **9**: 81-105, 1980
4) Irving TC, Konhilas J, Perry D, Fischetti R, de Tombe PP: Myofilament lattice spacing as a function of sarcomere length in isolated rat myocardium. Am J Physiol **279**: H2568-H2573, 2000
5) Huxley HE, Brown W: The low-angle X-ray diagram of vertebrate striated muscle and its behaviour during contraction and rigor. J Mol Biol **30**: 383-434, 1967
6) Huxley AF: Muscle structure and theories of contraction. Prog Biophys Biophys Chem **7**: 255-318, 1957
7) Huxley HE: Structural difference between resting and rigor muscle—evidence from intensity changes in the low-angle equatorial X-ray diagram. J Mol Biol **37**: 507-520, 1968
8) Haselgrove JC, Huxley HE: X-ray evidence for radial cross-bridge movement and for the sliding filament model in actively contracting skeletal muscle. J Mol Biol **77**: 549-568, 1973
9) Yagi N, Matsubara I: Equatorial X-ray reflections from contracting muscle after an applied stretch. Pflugers Arch **372**: 113-114, 1977
10) Matsubara I, Suga H, Yagi N: An X-ray diffraction study of the cross-circulated canine heart. J Physiol **270**: 311-320, 1977
11) Matsubara I, Kamiyama A, Suga H: X-ray diffraction study of contracting heart muscle. J Mol Biol **111**: 121-128, 1977
12) Matsubara I, Millman BM: X-ray diffraction patterns from mammalian heart muscle. J Mol Biol **82**: 527-536, 1974
13) Matsubara I, Yagi N, Endoh M: The state of cardiac contractile proteins during the diastolic phase. Jpn Circ J **46**: 44-48, 1982
14) Matsubara I, Yagi N, Endoh M: Behaviour of myosin projections during the staircase phenomenon of heart muscle. Nature **273**: 67, 1978
15) Matsubara I, Yagi N, Endoh M: Movement of myosin heads during a heart beat. Nature **278**: 474-476, 1979
16) Matsubara I, Yagi N, Endoh M: The states of myosin heads in heart muscle during systolic and diastolic phases. Eur Heart J Suppl A **1**: 17-20, 1980
17) Matsubara I, Maughan DW, Saeki Y, Yagi N: Cross-bridge movement in rat cardiac muscle as a function of calcium concentration. J Physiol **417**: 555-565, 1989
18) Matsubara I, Yagi N: A time resolved X-ray diffraction study of muscle during twitch. J Physiol **278**: 297-307, 1978
19) Yagi N, Saeki Y, Ishikawa T, Kurihara S: Cross-bridge and calcium behavior in ferret papillary muscle in different thyroid states. Jpn J Physiol **51**: 319-326, 2001
20) Okuyama H, Yagi N, Toyota H, Araki J, Iribe G, Imaoka T, Nakamura K, Simizu J, Kakisita M, Tsujioka K, Kajiya F, Suga H: Cardiac cross-bridge dynamics during shortening examined by X-ray diffraction. Proc of 16th Symposium on Biological and Physiological Engineering, Kitasato University, Kanagawa, Japan, 2001, 241-244
21) Taylor EW: Mechanism of actomyosin ATPase and the problem of muscle contraction. Sanadi D R, Packer L ed, Current Topics in Bioenergetics, Academic Press, New York, 1973, 201-231
22) Opie LH: Regulation of myocardial contractility. J Cardiovasc Pharmacol **26**: S1-S9, 1995
23) Kass DA, Hare JM, Georgakopoulos D: Murine cardiac function: A cautionary tail. Circ Res **82**: 519-522, 1998
24) James JF, Hewett TE, Robbins J: Cardiac physiology in transgenic mice. Circ Res **82**: 407-415, 1998
25) Suga H: Total mechanical energy of a ventricle model and cardiac oxygen consumption. Am J Physiol **236**: H498-H505, 1979

26) Suga H: Paul Dudley White International Lecture: cardiac performance as viewed through the pressure-volume window. Jpn Heart J **35**: 263-280, 1994

27) Suga H, Sagawa K, Shoukas AA: Load independence of the instantaneous pressure-volume ratio of the canine left ventricle and effects of epinephrine and heart rate on the ratio. Circ Res **32**: 314-322, 1973

28) Suga H, Sagawa K: Instantaneous pressure-volume relationships and their ratio in the excised, supported canine left ventricle. Circ Res **35**: 117-126, 1974

29) Suga H: End-systolic pressure-volume relations. Circulation **59**: 419-420, 1979

30) Suga H, Hayashi T, Shirahata M, Suehiro S, Hisano R: Regression of cardiac oxygen consumption on ventricular pressure-volume area in dog. Am J Physiol **240**: H320-H325, 1981

31) Suga H, Hayashi T, Shirahata M: Ventricular systolic pressure-volume area as predictor of cardiac oxygen consumption. Am J Physiol **240**: H39-H44, 1981

32) Suga H, Hayashi T, Suehiro S, Hisano R, Shirahata M, Ninomiya I: Equal oxygen consumption rates of isovolumic and ejecting contractions with equal systolic pressure-volume areas in canine left ventricle. Circ Res **49**: 1082-1091, 1981

33) Kass DA, Maughan WL: From 'E_{max}' to pressure-volume relations: a broader view. Circulation **77**: 1203-1212, 1988

34) Suga H: Ventricular energetics. Physiol Rev **70**: 247-277, 1990

35) Ito H, Takaki M, Yamaguchi H, Tachibana H, Suga H: Left ventricular volumetric conductance catheter for rats. Am J Physiol **270**: H1509-H1514, 1996

36) Tachibana H, Takaki M, Lee S, Ito H, Yamaguchi H, Suga H: New mechanoenergetic evaluation of left ventricular contractility in *in situ* rat hearts. Am J Physiol **272**: H2671-H2678, 1997

37) Khalafbeigui F, Suga H, Sagawa K: Left ventricular systolic pressure-volume area correlates with oxygen consumption. Am J Physiol **237**: H566-H569, 1979

38) Suga H, Goto Y, Futaki S, Kawaguchi O, Yaku H, Hata K, Takasago T: Systolic pressure-volume area (PVA) as the energy of contraction in Starling's law of the heart. Heart Vessels **6**: 65-70, 1991

39) Suga H, Taylor TW: Myocardial efficiency and economy in Huxley's 1957 crossbridge model. Jpn Heart J **32**: 827-834, 1991

40) Goto Y, Slinker BK, LeWinter MM: Decreased contractile efficiency and increased non-mechanical energy cost in hyperthyroid rabbit heart: Relation between O_2 consumption and systolic pressure-volume area or force-time integral. Circ Res **66**: 999-1011, 1990

41) Weisberg A, Winegrad S: Relation between crossbridge structure and actomyosin ATPase activity in rat heart. Circ Res **83**: 60-72, 1998

42) Sunagawa K, Maughan WL, Burkhoff D, Sagawa K: Left ventricular interaction with arterial load studied in isolated canine ventricle. Am J Physiol **245**: H773-H780, 1983

43) Baan J, Jong TT, Kerkhof PL, Moene RJ, van Dijk AD, van der Velde ET, Koops J: Continuous stroke volume and cardiac output from intraventricular dimensions obtained with impedance catheter. Cardiovasc Res **15**: 328-334, 1981

44) Baan J, van der Velde ET, de Bruin HG, Smeenk GJ, Koops J, van Dijk AD, Temmerman D, Senden J, Buis B: Continuous measurement of left ventricular volume in animals and humans by conductance catheter. Circulation **70**: 812-823, 1984

45) Abe S, Ohtomo J, Yamaguchi I, Tsuchida E, Fujinuma T, Sunagawa K, Tomoike H: Continuous measurement of left ventricular volume in rabbit, using a two-electrode catheter. Heart Vessels **10**: 138-145, 1995

46) Kass DA, Yamazaki T, Burkhoff D, Maughan WL, Sagawa K: Determination of left ventricular end-systolic pressure-volume relationships by the conductance (volume) catheter technique. Circulation **73**: 586-595, 1986

47) Georgakopoulos D, Mitzner WA, Chen C-H, Byrne BJ, Millar HD, Hare JM, Kass DA: In vivo murine left ventricular pressure-volume relations by miniaturized conductance micromanometry. Am J Physiol **274**: H1416-H1422, 1998

48) Feldman MD, Erikson JM, Mao Y, Korcarz CE, Lang RM, Freeman GL: Validation of a mouse conductance system to determine LV volume: comparison to echocardiography and crystals. Am J Physiol **279**: H1698-H1707, 2000

49) ter Keurs HE: Sarcomere function and crossbridge cycling. Adv Exp Med Biol **382**: 125-135, 1995

THE JOURNAL OF BIOLOGICAL CHEMISTRY

Vol. 277, No. 18, Issue of May 3, pp. 15286–15292, 2002
Printed in U.S.A.

Guanine Nucleotide Exchange Factor-like Factor (Rlf) Induces Gene Expression and Potentiates α_1-Adrenergic Receptor-induced Transcriptional Responses in Neonatal Rat Ventricular Myocytes*

Received for publication, December 12, 2001, and in revised form, February 1, 2002
Published, JBC Papers in Press, February 14, 2002, DOI 10.1074/jbc.M111844200

Ginell R. Post‡, Carol Swiderski, Bruce A. Waldrop, Lina Salty, Christopher C. Glembotski§, Rob M. F. Wolthuis¶‖, and Naoki Mochizuki**

*From the Department of Pharmaceutical Sciences, University of Kentucky, Lexington, Kentucky 40536, the §Department of Biology, San Diego State University, San Diego, California 92182, the ¶Department of Physiological Chemistry and Centre for Biomedical Genetics, University Medical Center Utrecht, 3584 CG Utrecht, The Netherlands, and the **Department of Structural Analysis, National Cardiovascular Center Research Institute, Fujishirodai 5-7-1, Suita, Osaka 565-8565, Japan*

Expression of constitutively active Ras (V12Ras) in cultured neonatal rat ventricular myocytes or targeted cardiac expression of V12Ras in transgenic mice induces myocardial cell growth and expression of genes that are markers of cardiac hypertrophy including atrial natriuretic factor (ANF) and myosin light chain-2. However, the signaling pathways that modulate the effects of Ras on acquisition of the various features of cardiac hypertrophy are not known. We identified the Ral guanine nucleotide exchange factor-like factor (Rlf) in a yeast two-hybrid screen of human heart cDNA library using Ras as bait, suggesting that Ras signaling in the heart may involve Rlf. We demonstrate here that Rlf is expressed in human heart. Expression of wild type Rlf or Rlf-CAAX, a membrane-targeted mutant of Rlf, transactivated ANF and myosin light chain-2 promoters but did not activate canonical cAMP responsive elements or phorbol ester responsive elements, suggesting that Rlf expression does not lead to a generalized increase in transcription. Transfection of mutant ANF promoter-reporter gene constructs demonstrated that the proximal serum response element is both necessary and sufficient for Rlf-inducible ANF expression. Rlf-induced ANF promoter activation required Ral and Cdc42 but not RhoA, Rac1, ERK, or p38 kinase activation. In addition, Rlf potentiated α_1-adrenergic receptor (α_1-AR)-induced ANF expression. Prolonged activation of the α_1-AR increases RalGTP levels in neonatal rat ventricular myocytes, further emphasizing a role for Ral guanine nucleotide exchange factors in α_1-AR signaling. Overall, this study supports the concept that Rlf and Ral are important previously unrecognized signaling components that regulate transcriptional responses in myocardial cells.

In response to hormones and mechanical stretch, ventricular myocytes exhibit a hypertrophic response characterized by induction of cardiac-specific genes (such as atrial natriuretic factor (ANF)[1] and myosin light chain (MLC-2)) and increased myocardial cell size (1). Expression of activated Ras (V12Ras) induces cellular hypertrophy and ANF expression in cultured neonatal rat ventricular myocytes (NRVMs) (2). Cardiac-targeted (MLC-2v-driven) expression of V12Ras induces cardiac hypertrophy and diastolic dysfunction in transgenic mice (3). Further studies conducted in NRVM indicate that transcriptional and morphological features of myocardial cell hypertrophy mediated by α_1-adrenergic (α_1-AR) and M_1 muscarinic cholinergic receptors require Ras activation (2, 4, 5). These observations imply an important role for Ras activation in development of cardiac hypertrophy; however, the role of specific Ras signaling pathways in cardiac hypertrophy has not been defined.

The best characterized effectors of Ras are serine/threonine kinases of the Raf family. Raf kinases regulate the activity of a kinase cascade that includes mitogen-activated/extracellular signal-regulated kinase kinase (MEK) and extracellular signal-regulated kinase (ERK) (6). The relative importance of the Ras-ERK pathway in cardiac hypertrophy is controversial. Some studies have shown that inhibition of ERK activation blocks α_1-AR-induced ANF expression in cultured cells (7, 8). Other studies using either transfection of dominant negative forms of Raf and ERK or pharmacological blockade of ERK indicate that Raf and ERK are not required for α_1-AR-induced increases in cell size (7) or ANF expression (9, 10). In support of the latter studies ERK activity is not elevated in the hearts of V12Ras transgenic mice, although significant ventricular hypertrophy is observed (10). Furthermore, whereas V12Ras induces myofilament disarray, cardiac fibrosis, and diastolic dysfunction in transgenic mice (3, 11), cardiac-targeted expression of activated MEK induces concentric hypertrophy and hyperdynamic contractile function, which is characteristic of

* This work was supported by an American Heart Association California affiliate grant-in-aid and a scientist development grant (to G. R. P.), an American Foundation for Pharmaceutical Education fellowship (to B. A. W.), and an American Heart Association student fellowship (to L. S.). The costs of publication of this article were defrayed in part by the payment of page charges. This article must therefore be hereby marked "*advertisement*" in accordance with 18 U.S.C. Section 1734 solely to indicate this fact.

‡ To whom correspondence should be addressed: University of Kentucky College of Pharmacy, Rose St., Lexington, KY 40536-0082. Tel.: 859-257-2633; Fax: 859-257-7564; E-mail: grpost@uky.edu.

‖ Present address: Wellcome/CRC Inst., Tennis Court Rd., Cambridge CB2 QR, UK.

[1] The abbreviations used are: ANF, atrial natriuretic factor; α_1-AR, α_1-adrenergic receptor; CRE, cAMP response element; ERK, extracellular signal-regulated kinase; GEF, guanine nucleotide exchange factor; JNK, c-Jun N-terminal kinase; MEK, mitogen-activated/ERK kinase; MLC-2, myosin light chain-2; NRVM, neonatal rat ventricular myocyte; PKC, protein kinase C; PI 3-kinase, phosphatidylinositol 3-kinase; Rlf, Ral guanine nucleotide exchange factor-like factor; PE, phenylephrine; TPA, 12-*O*-tetradecanoylphorbol-13-acetate; SRE, serum response element; TRE, TPA response element; GST, glutathione *S*-transferase; SFM, serum-free medium; V12Ras, constitutively active mutant of Ras; RalGDS, Ral guanine nucleotide dissociation stimulator.

compensated cardiac hypertrophy (12). The difference in cardiac phenotype between V12Ras and MEK transgenic mice may reflect the ability of V12Ras to activate additional signaling pathways that lead to impaired cardiac function (13).

In addition to Raf, Ras directly activates phosphatidylinositol 3-kinase (PI 3-kinase) and Ral guanine nucleotide exchange factors (RalGEFs), which activate the Ral. Several other putative Ras effectors have been described, including a GTPase-activating protein for Ras (RasGAP) (14), AF6 (15), protein kinase C ζ (16), and Rin (17). Of these, RasGAP and RalGEFs have been implicated in mediating transcriptional responses to Ras in NRVMs (18, 19). Ras also regulates c-Jun N-terminal kinase (JNK) and p38 kinase through activation of MEK kinase or the Rho-related G proteins Rac1 and Cdc42 (reviewed in Ref. 6). JNK and p38 kinases are activated by the α_1-AR agonist phenylephrine (PE) in NRVMs (20–22), and JNK is activated in hearts of V12Ras transgenic mice (10). Recent reports indicate that the balance between activation of ERK, JNK, and isoforms of p38 kinase may determine whether ventricular myocytes undergo hypertrophy or apoptosis (13, 22–25).

To understand the role of Ras signaling pathways in cardiac hypertrophy, we performed a yeast two-hybrid screen of a human heart cDNA library. This screen identified the human homologue of a protein previously shown to associate with the GTP-bound form of Ras and its close relative Rap1 (26, 27). The murine homologue, termed Rlf for Ral guanine nucleotide dissociation stimulator (RalGDS)-like factor, is a specific activator of Ral (28). In addition to interacting in the yeast two-hybrid system, Ras and Rlf interact as recombinant proteins in *in vitro* binding assays (29). In fibroblasts Rlf mediates Ras-induced transcriptional activation of the c-*fos* promoter through a pathway independent of Raf-MEK-ERK (30). The role of Rlf in cardiac hypertrophy has not been explored.

The aim of this study was to investigate the role of Rlf in transcriptional responses in NRVMs. We report that expression of either wild type or a membrane-targeted form of Rlf induces transcriptional activation of genes that are markers of cardiac hypertrophy but do not elicit a global effect on transcription. Rlf-mediated activation of the ANF promoter requires the proximal serum response element (SRE), Ral, and Cdc42 but not Rho, Rac, ERK, or p38 kinase activation. Consistent with a role for Ral guanine nucleotide exchange factors in hypertrophic signaling, Rlf potentiates the transcriptional response to α_1-AR activation. In addition Ral is activated following prolonged stimulation of the α_1-AR in NRVMs. These findings suggest that Rlf is an important previously unrecognized signaling component in myocardial cell growth responses.

EXPERIMENTAL PROCEDURES

Two-hybrid Screening—For library screening, the yeast reporter strain Y190 (obtained from Dr. S. Elledge, Baylor College of Medicine) was transformed with a bait plasmid that expressed a fusion protein between the Gal4 DNA binding domain and wild type human H-Ras, with a mutation of the membrane-targeting *CAAX* sequence to aid in nuclear localization. Ras-expressing yeast were isolated and transformed with 200 μg of human heart library inserted into pGAD10 (Matchmaker) according to the manufacturer's instructions (CLONTECH). Transformants capable of growth on synthetic media lacking uracil, leucine, tryptophan, and histidine containing 2 mM 3-aminotriazole were assayed for β-galactosidase activity using a filter lift assay. The vector pGAD10 containing potential Ras-interacting cDNAs were rescued from yeast and used to transform HB101 *Escherichia coli*. Two pGAD10 plasmids containing ~1.5-kb inserts were sequenced. BLAST searches revealed that one clone was identical to the Ras binding domain of human RGL2, a partial cDNA sequence identified as a Rap 1B-interacting protein and homologue of RalGDS (26). The second clone also overlapped the Ras binding region of RGL2. The full-length murine homologue of RGL2 was isolated and termed Rlf for Ral guanine nucleotide exchange factor-like factor (27).

Northern Analysis—RNA was prepared from several human tissues by the single-step guanidinium thiocyanate method. Twenty micrograms of total RNA was electrophoresed on a 1% agarose gel and blotted to nylon membrane. The Northern blot was processed using a previously described procedure (31). The 1.5-kb fragment of human RGL2 isolated in the yeast two-hybrid screen was excised from pGAD10 using *Eco*RI, and the fragment was used as a probe. Briefly, the membrane was hybridized with ^{32}P-labeled RGL2 or glyceraldehyde-3-phosphate dehydrogenase in 0.5 M sodium phosphate buffer containing 1% bovine serum albumin (fraction V) and 7% SDS at 65 °C. After overnight hybridization, the membrane was washed to a final stringency of 0.5× SSC/0.1% SDS at 40 °C for 5 min and exposed to film. The size of the transcripts was estimated by the migration of 28 S and 18 S ribosomal RNA.

Myocyte Isolation and Culture—Neonatal rat ventricular myocytes were prepared from hearts of 1–2 day old Sprague-Dawley rats as described previously (32). Briefly, ventricles were trisected and pooled, and cells were dissociated in collagenase and pancreatin solution prior to purification of NRVMs on a Percoll step gradient. NRVMs were plated at 4×10^4 cells/cm^2 on gelatin-coated plates and maintained in Dulbecco's modified Eagle's medium/medium 199 (Invitrogen) (4:1) containing 10% horse serum and 5% fetal calf serum for 24 h prior to experimentation.

Plasmids—The ANF reporter genes used in this study contain sequences of the 5′-flanking region of the rat ANF promoter cloned upstream of firefly luciferase cDNA (33). The ANF promoter mutants-luciferase reporter gene constructs have been previously described (34) and include ANF-638 (−638 to +65 base pairs of the rat ANF promoter fused upstream of the firefly luciferase gene), ANF-134 (containing −134 to +65 base pairs of the ANF promoter), a mutated form of the ANF-134 promoter that does not bind the serum response factor (M ANF SRE), ANF-65 (−65 to +65 base pairs of the ANF promoter), and ANF-65 (ANF SRE), contains sequences −125 to −102 of the ANF promoter fused to ANF-65. The MLC-2v reporter gene contains a 2.7-kb fragment of the MLC-2 promoter fused to luciferase cDNA (35). The expression plasmids encoding Rlf and Rlf-*CAAX* have been described (27, 30), and dominant interfering mutants of Rho, Rac, and Cdc42 were provided by Dr. Gary Bokoch (The Scripps Research Institute).

Transient Transfection and Reporter Gene Assays—For calcium phosphate transfection, myocytes were exposed to a cDNA-calcium phosphate precipitate 24 h after plating on 6-cm dishes as described (9). The amount of individual plasmid is indicated in the figure legend. Following transfection NRVMs were washed extensively and maintained in serum-free medium or incubated in the presence of 100 μM PE plus 2 μM propranolol (to block β-adrenergic receptors) for 48 h. Cells were harvested in a 0.5% Triton X-100 buffer, and luciferase activity and protein content of the lysate were determined for each sample as described (36). Luciferase activity was normalized to both cotransfected RSV-driven β-galactosidase reporter gene and protein content. Because the RSV promoter is sensitive to some stimuli used to induce hypertrophy (such as activated Ras) the data are presented as luciferase activity normalized to protein content in the cellular lysate.

Determination of Endogenous Ral Activation—Myocardial cells grown in 10-cm dishes were transfected with 1 μg/ml pMT2 (backbone vector) or RalV23 (a GTP hydrolysis-resistant mutant of Ral used as a positive control) by calcium phosphate precipitation. Transfected cells were washed and serum-starved overnight then treated with PE (100 μM) plus 2 μM propranolol or 15% serum for various times. A GST fusion protein that binds specifically to GTP-bound Ral (GST-RalBD) was prepared in *E. coli*, and endogenous Ral activation was measured as described (37). Briefly, myocardial cell lysates were prepared in Ral buffer (15% glycerol, 50 mM Tris, pH 7.4, 1% Nonidet P-40, 200 mM NaCl, 5 mM $MgCl_2$, and protease inhibitors) and then incubated with GST-RalBD for 1 h at 4 °C. Pellets were washed, and bound RalGTP were separated by 12% SDS-PAGE and detected by Western blotting with a monoclonal anti-RalA antibody (Transduction Labs) and chemiluminescence. Autoradiograms were quantified by densitometry or chemiluminescent imaging (Molecular Dynamics).

RESULTS

Yeast Two-hybrid System Identifies Rlf as a Ras-interacting Protein in the Heart—To identify proteins that interact with Ras and therefore contribute to Ras-induced myocardial cell growth, we used the yeast two-hybrid system. We screened a human heart cDNA library (10^7 independent clones, CLONTECH) using Ras with a mutated *CAAX* sequence as bait. We obtained two clones that displayed growth on His$^-$ plates and

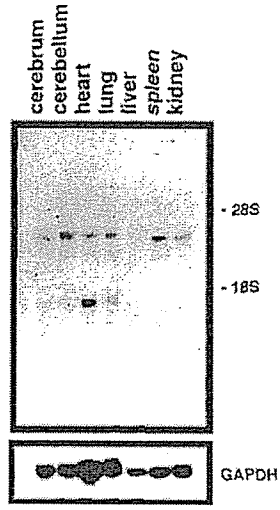

FIG. 1. **Northern blot analysis of Rlf.** Twenty micrograms of total RNA from human tissue was analyzed by Northern blot. The blot was hybridized with an Rlf probe or a randomly primed glyceraldehyde-3-phosphate dehydrogenase fragment (*lower panel*).

β-galactosidase activity. Sequencing of the cDNA revealed that one clone was identical to the Ras binding domain of human RGL2, a partial cDNA sequence identified as a homologue of RalGDS (26). The second clone also overlapped the Ras binding region of RGL2. The full-length murine homologue of RGL2 was identified as a Rap 1A-binding protein and was termed Rlf (27).

Expression of Rlf in Human Tissues—To investigate the pattern of expression of RGL2 in various tissues we performed Northern analysis using the 1.5-kb fragment of RGL2 isolated in the yeast two-hybrid screen with total RNA prepared from adult human tissues. In agreement with the predicted size of the full-length Rlf transcript (27), a transcript of ~3 kb was detected in the heart, brain, lung, spleen, and kidney (Fig. 1). Despite equal amounts of total RNA (determined by optical density), glyceraldehyde-3-phosphate dehydrogenase levels were modestly higher in heart and lung tissue. Furthermore, an additional smaller transcript was detected in the heart. This smaller transcript may represent another RalGDS homologue, a splice variant of Rlf, or a related mRNA. Nonetheless, the expression of RGL2 in the human heart and its ability to interact with Ras in the yeast two-hybrid system suggests that RGL2 may be an important component of Ras signaling in myocardial cells.

Rlf Activates the ANF and MLC-2 Promoters in Cardiac Myocytes—Expression of Ras mutants that preferentially activate Raf and RalGEFs up-regulates genes associated with cardiac hypertrophy and increases myocardial cell size, suggesting that exchange factors for Ral are important regulators of Ras-induced cardiac hypertrophy (19). To examine the role of Rlf in cardiac-selective gene expression, NRVMs were transiently transfected with the cDNA for wild type Rlf together with ANF or MLC-2 promoter-luciferase constructs and maintained in serum-free medium. Targeting of Rlf to the plasma membrane by replacement of the C-terminal Ras binding domain with the Ras membrane localization signal (*CAAX*) eliminates the requirement for Ras binding in activation (30). We tested the effect of wild type Rlf and Rlf-*CAAX* on the induction of ANF and MLC-2 promoter activity. As shown in Fig. 2, expression of either wild type Rlf or Rlf-CAAX is sufficient to activate ANF and MLC-2 promoter-luciferase reporter genes. Expression of the Rlf-CAAX construct in which a large region of the Ral guanine nucleotide exchange domain was deleted (Rlf-ΔCAT-CAAX) (30) did not induce ANF promoter activity (not shown), indicating that the ability of Rlf to induce nucleotide exchange on Ral is required for transcriptional activation of cardiac-specific genes.

The promoter of the ANF gene contains regulatory sequence elements that function as binding sites for a variety of transcription factors. In parallel experiments, we tested the effect of Rlf on induction of promoter-luciferase reporter genes containing cAMP responsive elements (CREs) or phorbol ester (TPA) responsive elements (TREs) (Fig. 2). In contrast to its effects on the ANF and MLC-2 promoters, expression of Rlf or Rlf-*CAAX* did not transactivate reporter genes driven by tandem repeats of canonical CREs or containing AP-1 binding sites (2× TRE). This observation indicates that Rlf does not induce a generalized effect on gene transcription in ventricular myocytes.

The SRE Is Necessary and Sufficient for Rlf-mediated ANF Expression—In previous studies it has been shown that nearly all information for α_1-AR-induction of ANF transcription resides in the 638-base pair region just 5′ to the transcriptional start site (38). In addition to CRE- and TRE-like sequences, this region of the ANF promoter contains two SREs. To further examine sequences present in the ANF promoter required for Rlf-mediated transcriptional regulation of ANF, we used a series of truncated and mutated ANF promoter luciferase constructs (34). NRVMs were transfected with backbone vector (pMT2) or Rlf and maintained in serum-free medium for 48 h prior to determination of luciferase activity. As shown in Fig. 3, Rlf-induced luciferase activity was similar in cells transfected with reporter plasmids containing either 638 or 134 base pairs of the 5′-flanking sequence of the ANF promoter. However, deletion of sequences between −134 and −65 abolished Rlf-stimulated ANF promoter activity, indicating that Rlf-responsive elements are situated between −134 and −65 base pairs of the ANF promoter. This region of the ANF promoter contains an SRE-like sequence without a 3′ Ets binding motif (38). To evaluate whether the ANF SRE is necessary for Rlf-mediated ANF induction, a mutation that disrupts serum response factor binding to the SRE was tested (ANF 134 (M ANF SRE)). Rlf did not transactivate this mutated ANF promoter-reporter construct. When the ANF SRE was inserted 5′ to the minimal ANF 65 promoter (ANF 65 (ANF SRE)), full responsiveness to Rlf was regained (Fig. 3). These results suggest that the SRE is necessary and sufficient for Rlf-inducible ANF expression.

Pharmacological Inhibitors of ERK Activation and p38 Kinase Activity Do Not Block Rlf-mediated ANF Expression—The mitogen-activated protein kinase family members (ERK, JNK, and p38 kinase) mediate transcriptional activation induced by a variety of hypertrophic agents. To test for the involvement of ERK in Rlf-induced ANF expression, Rlf- and backbone-transfected myocardial cells were treated with the cell-permeable inhibitor of ERK activation (39) or Me_2SO for 48 h. At a concentration (10 μM) that inhibits α_1-AR-induced ERK activation (9), the MEK inhibitor did not inhibit Rlf-induced ANF expression (Fig. 4). The lack of inhibition by PD98059 was consistent with a previous study showing that Rlf-induced c-*fos* expression occurs through an ERK-independent pathway in fibroblasts (30).

The ANF SRE is activated by p38 kinase (34). To determine whether p38 kinase mediates the transcriptional responses of Rlf in myocardial cells, we examined Rlf-induced activation of the ANF promoter in the presence of 5 μM SB 203580, a selective inhibitor of p38 α/β kinases (40). Although this concentration of SB 203580 blocks PE-induced ATF6-induced transcriptional responses (Ref. 34 and data not shown), SB 203580 did not block Rlf-induced ANF expression (Fig. 4). Together, these

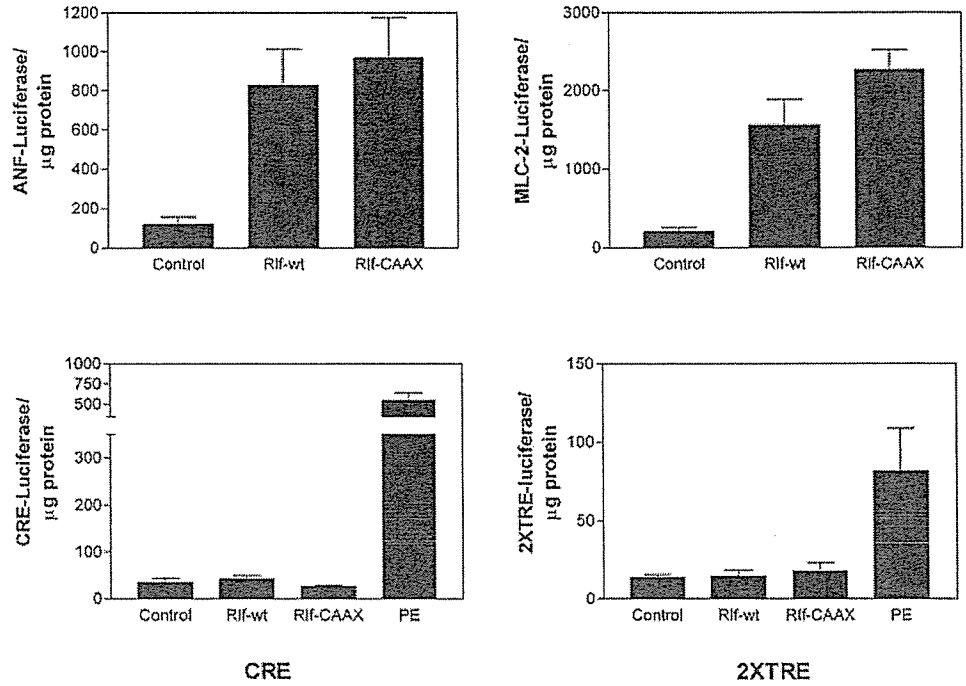

FIG. 2. **Rlf and Rlf-CAAX stimulate transcription activation of the ANF and MLC-2 promoter but do not lead to generalized increases in gene expression.** Myocardial cells were cotransfected with 5 µg of the cDNA-encoding backbone vector (pMT2), wild type Rlf (*Rlf-wt*), a membrane-targeted Rlf (*Rlf-CAAX*) together with 3 µg of the ANF3003 promoter-luciferase construct, the MLC-2 reporter gene, a cAMP response element (*CRE*), or a phorbol ester responsive element (*2XTRE*). Cells were maintained in serum-free medium (SFM) for backbone, Rlf, and Rlf-CAAX-transfected cells or treated with the α_1-AR agonist phenylephrine (100 µM) plus 2 µM propranolol (to block β-AR) for 48 h. Luciferase activity in cell lysates was determined, and results were normalized to protein content. Data are the mean ± S.E. of three experiments performed in triplicate.

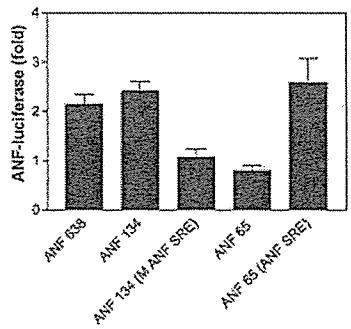

FIG. 3. **The SRE is necessary and sufficient for Rlf-inducible ANF expression.** Myocytes were transfected with 5 µg of wild type Rlf or backbone vector (pMT2) together with a series of truncated and mutated ANF promoter-luciferase constructs. The ANF-638, ANF-134, and ANF-65 promoter constructs contain 638, 134, or 65 base pairs of the 5′-flanking region of the rat ANF promoter, respectively. ANF-134 (M ANF SRE) is the ANF-134 promoter with a mutation that disrupts binding of the serum response factor to the SRE. The ANF-65 (ANF SRE) contains the ANF SRE inserted 5′ to the ANF-65 base pair promoter. Myocytes were maintained in SFM for 48 h, and luciferase activity was determined and normalized to protein content. Data expressed are the average-fold activation induced by Rlf relative to control ± S.E. from three experiments performed in triplicate.

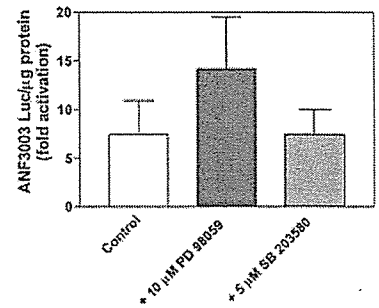

FIG. 4. **Inhibitors of ERK or p38 kinase activity do not block Rlf-induced activation of the ANF promoter.** Myocytes were transfected with 2 µg of wild type Rlf or backbone vector (pMT2) and the full-length ANF promoter. Transfected cells were washed and then incubated with either Me_2SO (0.1%; control), 10 µM PD98059, or 5 µM SB 203580 for an additional 48 h. Luciferase activity was determined and normalized to protein content. Data are expressed as fold activation mean ± S.E. of four experiments performed in triplicate.

results demonstrate that activation of ERK and p38 α/β kinase is not required for transcriptional effects of Rlf.

Dominant Negative Ral Blocks Rlf-induced Activation of the ANF Promoter—We investigated the role of Ral in Rlf-induced ANF expression by co-expressing RalN28, a dominant negative mutant of Ral (DNRal) that is constitutively GDP-bound (30). As shown in Fig. 5, DNRal inhibited Rlf-induced ANF promoter activity. This result implies that Ral mediates Rlf-induced activation of the ANF promoter.

Dominant Negative Cdc42, but Not Rac or Rho, Blocks Rlf-induced Activation of the ANF Promoter—The Rho family of G proteins (RhoA, Rac1, and Cdc42) regulates transcriptional activation by the serum response factor and the SRE through mitogen-activated protein kinase-independent pathways (41). To investigate the role of Rho-related G proteins in Rlf-induced ANF expression, NRVMs were transfected with Rlf alone or with dominant negative mutants of either RhoA (N19RhoA), Rac (N17Rac1), or Cdc42 (N17Cdc42). Expression of N17Cdc42 but not N17Rac or N19Rho attenuated Rlf-induced ANF expression (Fig. 6). This result suggests that Cdc42 is required for Rlf-induced ANF gene expression.

Rlf Enhances α_1-AR-induced ANF Promoter Activation—To examine the role of Rlf in α_1-AR-mediated activation of the

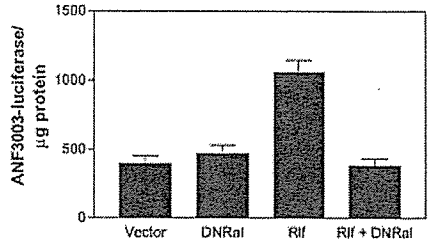

FIG. 5. **Dominant interfering mutant of Ral blocks Rlf-induced ANF expression.** NRVMs were transfected with Rlf (5 μg) or backbone vector (pMT2) together with 3 μg of dominant negative Ral (*DNRal*) and the ANF3003 promoter-luciferase reporter gene. Cells were incubated in SFM for 48 h prior to determination of ANF luciferase activity and protein content. Data are the mean ± S.E. of three experiments performed in triplicate.

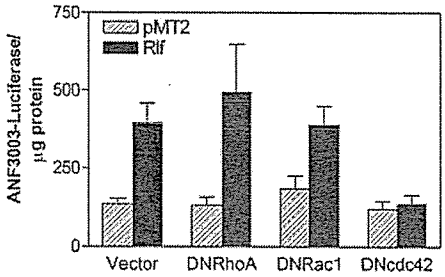

FIG. 6. **Dominant interfering mutant of Cdc42 blocks Rlf-induced ANF expression.** NRVMs were cotransfected with Rlf (5 μg) or backbone vector (pMT2) together with 3 μg of pCMV5 or dominant negative RhoA (*DNRhoA*), Rac1 (*DNRac1*), or Cdc42 (*DNCdc42*) and the ANF3003 promoter-luciferase reporter gene. Cells were incubated in SFM for 48 h prior to determination of ANF luciferase activity and protein content. Data are the mean ± S.E. of four experiments performed in triplicate.

ANF promoter, myocardial cells were transfected with backbone vector (pMT2) or wild type Rlf (5 μg) together with the ANF reporter gene construct. Cells were then incubated in the presence or absence of the α_1-AR agonist PE (100 μM) and propranolol (2 μM) for 48 h (to block endogenous β-adrenergic receptors). Activation of the ANF promoter by PE was enhanced in Rlf-transfected cells (Fig. 7), suggesting that PE and Rlf activate sequential signaling pathways that converge on the ANF promoter. Alternatively, Rlf expression may be limiting for activation of the ANF promoter and thus increasing expression of Rlf enhances α_1-AR-Rlf signaling in myocardial cells.

PE Activates Ral—To examine PE-induced regulation of endogenous Ral in ventricular myocytes we used an affinity precipitation assay for activated Ral (37). Myocytes were treated with PE or 15% serum for 5 min to 24 h, and GTP-Ral was isolated from cell lysates using a GST-Ral binding domain fusion protein. The bound proteins were immunoblotted with an anti-Ral A antibody (Fig. 8). In contrast to serum-treated myocardial cells, Ral activation in PE-treated cells was detected at 24 h. Western blots of whole cell lysates indicate that PE-mediated increases in RalGTP at 24 h were not associated with an increase in Ral protein levels.

DISCUSSION

Despite numerous studies in NRVMs and transgenic mouse models of cardiac hypertrophy, the signaling cascade linking G protein-coupled receptors to activation of Ras and the role of Ras effectors in induction of genetic and morphologic changes characteristic of cardiac hypertrophy remains uncertain. Although α_1-AR-induced cardiac gene expression and changes in morphology require Ras activity (2), earlier studies suggested

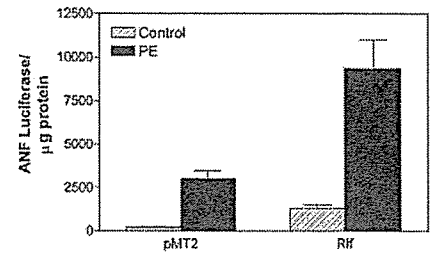

FIG. 7. **Wild type Rlf and α_1-AR activation synergize to activate the ANF promoter.** NRVMs were transfected with 5 μg of wild type Rlf or backbone vector (pMT2) together with the ANF reporter construct. Myocytes were maintained in SFM (*Control*) or in the presence of phenylephrine (*PE*) for 48 h. Luciferase activity was determined and normalized to protein content. Data are the mean ± S.E. from three experiments performed in triplicate.

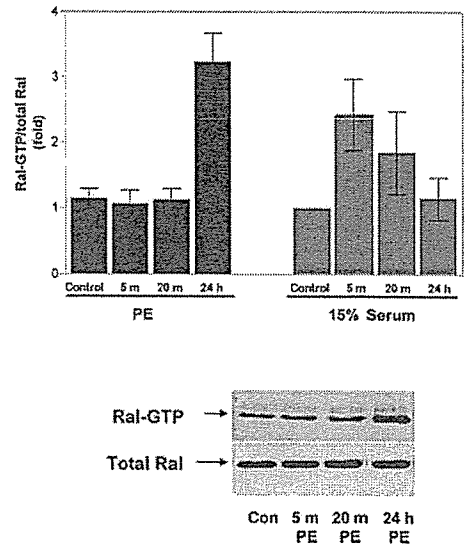

FIG. 8. **Stimulation of myocytes with PE induces delayed activation of Ral.** NRVMs transfected with pMT2 (3 μg) were untreated (*Control*) or stimulated with PE or 15% serum for 5 min, 20 min, or 24 h. Cells were lysed, and cellular lysates were incubated with GST-RalBD coupled to glutathione to isolate GTP-bound Ral. Beads were washed, and GTP-bound Ral was identified by Western analysis using a monoclonal antibody to Ral. Total Ral in cellular lysates was examined in separate Western blots for each experimental point. Total and GTP-bound Ral were quantitated from autoradiograms by densitometry or phosphorimaging. Data are the mean ± S.E. from three experiments performed in duplicate. A representative blot for PE-induced GTP-bound Ral (*top*) and total Ral (*bottom*) is shown.

that activation of the Raf-ERK kinase cascade is not sufficient to induce cardiac gene expression in ventricular myocytes or Ras transgenic mice (9, 10). These findings indicate that activation of additional Ras effectors is necessary for the characteristic changes in gene expression that occur in response to hypertrophic agonists or Ras. In agreement Fuller *et al.* (19) demonstrated that effector domain mutants of Ras that preferentially activate Raf and RalGEFs but not PI 3-kinase induce genes associated with the hypertrophic response in NRVMs (19), suggesting that RalGEF family members and their signaling pathways are important regulators of Ras-induced cardiac hypertrophy.

To identify potentially novel effector molecules of Ras in the heart, we screened a human heart cDNA library by the yeast two-hybrid system using Ras, and we identified the human homologue of Rlf as a Ras-interacting protein *in vitro* (27, 29). Rlf is a member of the family of Ras-binding proteins that function as RalGEFs (27). Other members of this family in-

clude RalGDS (42), Rgl (43), and RPM/RGL3 (44, 45). The biological role of RalGEFs in gene expression and cell growth is just beginning to be elucidated. When transfected into fibroblasts, Rlf mediates Ras-induced c-*fos* gene induction through a signaling pathway distinct from the Raf-MEK-ERK pathway (27, 30). Similarly, expression of RalGDS complements the activities of Raf and PI 3-kinase on cell growth and transformation in NIH3T3 fibroblasts (46). However, in PC12 cells expression of RalGDS opposes the action of Raf and PI 3-kinase and inhibits neurite outgrowth (47). Expression of RalGDS also inhibits expression of muscle-specific reporter genes and differentiation of C3H10T1/2 mouse fibroblasts to skeletal muscle (48). We show that Rlf is expressed in the heart (Fig. 1), induces the expression of genes associated with cardiac hypertrophy (Fig. 2), and potentiates the transcriptional response to PE (Fig. 7). Therefore, Rlf may play a role in regulating hypertrophic growth signals in terminally differentiated cardiac myocytes.

Induction of ANF is one of the most conserved features of the hypertrophic response. The promoter of the ANF gene contains several regulatory sequence elements that bind a variety of transcription factors. Using a series of truncated and chimeric ANF promoter-reporter gene constructs, we found that Rlf does not transactivate promoters containing canonical CREs and TREs. Furthermore, deletion of these regulatory motifs in the ANF promoter does not affect Rlf-mediated transcriptional activity. In contrast, the proximal SRE is both necessary and sufficient for Rlf-mediated transactivation of the ANF promoter (Fig. 3). This region of the promoter is a target for multiple intracellular signaling pathways in myocardial cells, including p38 kinase (34, 49), calcium calmodulin kinase (50), electrical pacing (51), RhoA, and the protein kinase C (PKC)-related kinase PKN (52). We found that Rlf-induced transcriptional activation of the ANF promoter requires Ral and Cdc42 but not Rho, Rac, ERK, or p38 kinase activation. An earlier study using transfection of dominant inhibitory and activated RhoA and Ras suggests that RhoA transactivates the ANF promoter through a pathway that is parallel and complementary to Ras (53). The interrelationship between Ras, Ral, Rac, and Cdc42 with respect to hypertrophic growth responses in myocardial cells has not been established. However, our data are consistent with a model that places Rlf on a pathway parallel to both RhoA and Rac.

An important function of Rho-related G proteins is control of actin polymerization and the assembly of integrin complexes. In addition to its impact on cellular morphology and movement, actin polymerization and/or stabilization induce the expression of SRE target genes (54). A recent study has shown that RhoA-mediated organization of the actin cytoskeleton facilitates hypertrophic gene induction (55). Like the Rho family of G proteins, Ral has been linked to changes in cellular morphology. For example, expression of a dominant-interfering mutant of Ral blocks developmental shape changes in *Drosophila melanogaster* (56) whereas activated Ral induces filopodial outgrowth in fibroblasts (57). A link between Rlf and the actin cytoskeleton is formed through Ral and an effector protein of Ral, Ral-binding protein 1 (RalBP1). RalBP1 binds to Cdc42 and Rac through a GTPase domain (58). Together Rlf signaling to the SRE may involve Ral and/or Cdc42-induced regulation of actin polymerization, an area of investigation that we are actively pursuing.

The regulation of RalGEF activity is just beginning to be elucidated. Several G protein-coupled receptors and receptor tyrosine kinases induce rapid and transient activation of Ral (37, 59, 60). Studies have demonstrated that insulin and EGF-induced Ral activation in fibroblasts is blocked by dominant negative Ras, providing evidence that the RalGEF-Ral pathway is downstream of Ras (60). Ral can also be activated through Ras-independent pathways involving calcium (37, 59). In addition, the activity of RalGDS can be negatively regulated by phorbol esters (61). We show here for the first time that α_1-ARs are coupled to signaling pathways that increase the levels of GTP-bound Ral. Although serum-induced Ral activation peaks at 5 min, PE-induced Ral activation occurs only following prolonged PE exposure (24 h). This contrasts with the kinetics of PE-induced ERK activation, which peaks at 5–20 min, returns to basal levels at 1 h, and remains low for 24 h (9). In a similar fashion, nerve growth factor-induced PKC activation enhanced ERK signaling and prevented Ras-mediated activation of RalGEF (61). Whether PKC mediates α_1-AR-induced activation of ERK and/or Ral in NRVMs is not known. However, our findings are consistent with a model whereby prolonged exposure to PE (24 h) down-regulates a pathway that inhibits RalGEF activation (such as PKC or RalGAP) or up-regulates an activator of Ral (possibly Rlf). In support of the latter mechanism, we found that Rlf overexpression enhances PE-induced ANF promoter activity (Fig. 7). The significance of Rlf expression and delayed Ral activation on myocardial cell hypertrophy is currently under investigation.

In summary, we identified the human homologue of Rlf as a Ras-interacting protein in the heart using the yeast two-hybrid system and demonstrated its expression in human heart. Expression of wild type and membrane-targeted Rlf is sufficient to activate the promoters of genes that are markers of cardiac hypertrophy but does not lead to generalized increases in gene expression in myocardial cells. Our studies show that Rlf-mediated transcriptional regulation of the ANF promoter requires Ral, Cdc42, and the proximal SRE but not ERK, p38 kinase, Rac1, or RhoA. Co-expression of Rlf and treatment of myocardial cells with PE enhances ANF promoter activity. We also show that PE increases RalGTP levels, further emphasizing a role for Rlf and Ral in α_1-AR signal transduction. Overall, these findings also suggest that Rlf and Ral signaling may be an important determinant in the development of myocardial hypertrophy.

Acknowledgments—We thank Dr. Paul Insel for his encouragement and support. We also thank Drs. Kirk Knowlton and Gary Bokoch for cDNA constructs used in this study, Drs. Douglas Andres, Steven Post, and Lisa Cassis for their comments on this manuscript, and Mahmoud Itani, Brian Torres, and Leah Allen for excellent technical assistance.

REFERENCES

1. Chien, K. R., Knowlton, K. U., Zhu H., and Chien S. (1991) *FASEB J.* **5**, 3037–3046
2. Thorburn, A., Thorburn, J., Chen, S. Y., Powers, S., Shubeita, H. E., Feramisco, J. R., and Chien, K. R. (1993) *J. Biol. Chem.* **268**, 2244–2249
3. Hunter, J. J., Tanaka, N., Rockman, H. A., Ross, J., Jr., and Chien, K. R. (1995) *J. Biol. Chem.* **270**, 23173–23178
4. Ramirez, M. T., Post, G. R., Sulakhe, P. V., and Brown, J. H. (1995) *J. Biol. Chem.* **270**, 8446–8451
5. Brown, J. H., Sah, V., Moskowitz, S., Ramirez, T., Collins, L., Post, G., and Goldstein, D. (1997) *Life Sci.* **60**, 1077–1084
6. Widmann, C., Gibson, S., Jarpe, M. B., and Johnson, G. L. (1999) *Physiol. Rev.* **79**, 143–180
7. Thorburn, J., Frost, J. A., and Thorburn, A. (1994) *J. Cell Biol.* **126**, 1565–1572
8. Glennon, P. E., Kaddoura, S., Sale, E. M., Sale, G. J., Fuller, S. J., and Sugden, P. H. (1996) *Circ. Res.* **78**, 954–961
9. Post, G. R., Goldstein, D., Thuerauf, D. J., Glembotski, C. C., and Brown, J. H. (1996) *J. Biol. Chem.* **271**, 8452–8457
10. Ramirez, M. T., Sah, V. P., Zhao, X. L., Hunter, J. J., Chien, K. R., and Brown, J. H. (1997) *J. Biol. Chem.* **272**, 14057–14061
11. Karlon, W. J., Covell, J. W., McCulloch, A. D., Hunter, J. J., and Omens, J. H. (1998) *Anat. Rec.* **252**, 612–625
12. Bueno, O. F., De Windt, L. J., Tymitz, K. M., Witt, S. A., Kimball, T. R., Klevitsky, R., Hewett, T. E., Jones, S. P., Lefer, D. J., Peng, C. F., Kitsis, R. N., and Molkentin, J. D. (2000) *EMBO J.* **19**, 6341–6350
13. Wang, Y. (2001) *Curr. Opin. Pharmacol.* **1**, 134–140
14. Yatani, A., Okabe, K., Polakis, P., Halenbeck, R., McCormick, F., and Brown, A. M. (1990) *Cell* **61**, 769–776
15. Van Aelst, L., White, M. A., and Wigler, M. H. (1994) *Cold Spring Harbor Symp. Quant. Biol.* **59**, 181–186
16. Diaz-Meco, M. T., Lozano, J., Municio, M. M., Berra, E., Frutos, S., Sanz, L.,

and Moscat, J. (1994) *J. Biol. Chem.* **269,** 31706–31710
17. Han, L., Wong, D., Dhaka, A., Afar, D., White, M., Xie, W., Herschman, H., Witte, O., and Colicelli, J. (1997) *Proc. Natl. Acad. Sci. U. S. A.* **94,** 4954–4959
18. Abdellatif, M., and Schneider, M. D. (1997) *J. Biol. Chem.* **272,** 525–533
19. Fuller, S. J., Finn, S. G., Downward, J., and Sugden, P. H. (1998) *Biochem. J.* **335,** 241–246
20. Bogoyevitch, M. A., Ketterman, A. J., and Sugden, P. H. (1995) *J. Biol. Chem.* **270,** 29710–29717
21. Lazou, A., Sugden, P. H., and Clerk, A. (1998) *Biochem. J.* **332,** 459–465
22. Zechner, D., Thuerauf, D. J., Hanford, D. S., McDonough, P. M., and Glembotski C. C. (1997) *J. Cell Biol.* **139,** 115–127
23. Wang, Y., Huang, S., Sah, V. P., Ross, J., Jr., Brown, J. H., Han, J., and Chien, K. R. (1998) *J. Biol. Chem.* **273,** 2161–2168
24. Nemoto, S., Sheng, Z., and Lin, A. (1998) *Mol. Cell. Biol.* **18,** 3518–3526
25. Zechner, D., Craig, R., Hanford, D. S., McDonough, P. M., Sabbadini, R. A., and Glembotski, C. C. (1998) *J. Biol. Chem.* **273,** 8232–8239
26. Peterson, S. N., Trabalzini, L., Brtva, T. R., Fischer, T., Altschuler, D. L., Martelli, P., Lapetina, E. G., Der, C. J., and White, G. C., II (1996) *J. Biol. Chem.* **271,** 29903–29908
27. Wolthuis, R. M., Bauer, B., van't Veer, L. J., de Vries-Smits, A. M., Cool, R. H., Spaargaren, M., Wittinghofer, A., Burgering, B. M., and Bos, J. L. (1996) *Oncogene* **13,** 353–362
28. Murai, H., Ikeda, M., Kishida, S., Ishida, O., Okazaki-Kishida, M., Matsuura, Y., and Kikuchi, A. (1997) *J. Biol. Chem.* **272,** 10483–10490
29. Mochizuki, N., Murakami, T., Sawa, H., Post, G. R., and Makita, N. (1997) *Circulation* **96,** I-556
30. Wolthuis, R. M., de Ruiter, N. D., Cool, R. H., and Bos, J. L. (1997) *EMBO J.* **16,** 6748–6761
31. Church, G. M., and Gilbert, W. (1984) *Proc. Natl. Acad. Sci. U. S. A.* **81,** 1991–1995
32. Iwaki, K., Sukhatme, V. P., Shubeita, H. E., and Chien, K. R. (1990) *J. Biol. Chem.* **265,** 13809–13817
33. Knowlton, K. U., Baracchini, E., Ross, R. S., Harris, A. N., Henderson, S. A., Evans, S. M., Glembotski, C. C., and Chien, K. R. (1991) *J. Biol. Chem.* **266,** 7759–7768
34. Thuerauf, D. J., Arnold, N. D., Zechner, D., Hanford, D. S., DeMartin, K. M., McDonough, P. M., Prywes, R., and Glembotski, C. C. (1998) *J. Biol. Chem.* **273,** 20636–20643
35. Henderson, S. A., Spencer, M., Sen, A., Kumar, C., Siddiqui, M. A., and Chien, K. R. (1989) *J. Biol. Chem.* **264,** 18142–18148
36. Shubeita, H. E., Martinson, E. A., Van Bilsen, M., Chien, K. R., and Brown, J. H. (1992) *Proc. Natl. Acad. Sci. U. S. A.* **89,** 1305–1309
37. Wolthuis, R. M., Franke, B., van Triest, M., Bauer, B., Cool, R. H., Camonis, J. H., Akkerman, J. W., and Bos, J. L. (1998) *Mol. Cell. Biol.* **18,** 2486–2491
38. Sprenkle, A. B., Murray, S. F., and Glembotski, C. C. (1995) *Circ. Res.* **77,** 1060–1069
39. Dudley, D. T., Pang, L., Decker, S. J., Bridges, A. J., and Saltiel, A. R. (1995) *Proc. Natl. Acad. Sci. U. S. A.* **92,** 7686–7689
40. Cuenda, A., Cohen, P., Buee-Scherrer, V., and Goedert, M. (1997) *EMBO J.* **16,** 295–305
41. Hill, C. S., Wynne, J., and Treisman, R. (1995) *Cell.* **81,** 1159–1170
42. Hofer, F., Fields, S., Schneider, C., and Martin, G. S. (1994) *Proc. Natl. Acad. Sci. U. S. A.* **91,** 11089–11093
43. Kikuchi, A., Demo, S. D., Ye, Z. H., Chen, Y. W., and Williams, L. T. (1994) *Mol. Cell. Biol.* **14,** 7483–7491
44. Shao, H., and Andres, D. A. (2000) *J. Biol. Chem.* **275,** 26914–26924
45. Ehrhardt, G. R., Korherr, C., Wieler, J. S., Knaus, M., and Schrader, J. W. (2001) *Oncogene* **20,** 188–197
46. White, M. A., Vale, T., Camonis, J. H., Schaefer, E., and Wigler, M. H. (1996) *J. Biol. Chem.* **271,** 16439–16442
47. Gob, T., Rusanescu, G., Urano, T., and Feig, L. A. (1999) *Mol. Cell. Biol.* **19,** 1731–1741
48. Ramocki, M. B., White, M. A., Konieczny, S. F., and Taparowsky, E. J. (1998) *J. Biol. Chem.* **273,** 17696–17701
49. Hines, W. A., Thorburn, J., and Thorburn, A. (1999) *Mol. Cell. Biol.* **19,** 1841–1852
50. Ramirez, M. T., Zhao, X. L., Schulman, H., and Brown, J. H. (1997) *J. Biol. Chem.* **272,** 31203–31208
51. McDonough, P. M., Hanford, D. S., Sprenkle, A. B., Mellon, N. R., and Glembotski, C. C. (1997) *J. Biol. Chem.* **272,** 24046–24053
52. Morissette, M. R., Sah, V. P., Glembotski, C. C., and Brown, J. H. (2000) *Am. J. Physiol.* **278,** H1769–H1774
53. Sah, V. P., Hoshijima, M., Chien, K. R., and Brown, J. H. (1996) *J. Biol. Chem.* **271,** 31185–31190
54. Sotiropoulos, A., Gineitis, D., Copeland, J., and Treisman, R. (1999) *Cell* **98,** 159–169
55. Wei, L., Wang, L., Carson, J. A., Agan, J. E., Imanaka-Yoshida, K., and Schwartz, R. J. (2001) *FASEB J.* **15,** 785–796
56. Sawamoto, K., Yamada, C., Kishida, S., Hirota, Y., Taguchi, A., Kikuchi, A., and Okano, H. (1999) *Oncogene* **18,** 1967–1974
57. Ohta, Y., Suzuki, N., Nakamura, S., Hartwig, J. H., and Stossel, T. P. (1999) *Proc. Natl. Acad. Sci. U. S. A.* **96,** 2122–2128
58. Feig, L. A., Urano, T., and Cantor, S. (1996) *Trends Biochem. Sci.* **21,** 438–441
59. Hofer, F., Berdeaux, R., and Martin, G. S. (1998) *Curr. Biol.* **8,** 839–842
60. Wolthuis, R. M., Zwartkruis, F., Moen, T. C., and Bos, J. L. (1998) *Curr. Biol.* **8,** 471–474
61. Rusanescu, G., Gotoh, T., Tian, X., and Feig, L. A. (2001) *Mol. Cell. Biol.* **21,** 2650–2658

Annual Report of Iwate Medical University
School of Liberal Arts and Sciences
No. 37(2002), 13-22.

New x-ray irradiation from weakly ionized linear plasma

Eiichi Sato[a], Yasuomi Hayasi[b], Rudolf Germer[c], Etsuro Tanaka[d], Hidezo Mori[e], Haruo Obara[f], Toshio Ichimaru[g] and Kazuyoshi Takayama[h]

(Received October 18, 2002)

ABSTRACT

In the plasma flash x-ray generator, high-voltage main condenser of about 200 nF is charged up to 50 kV by a power supply, and electric charges in the condenser are discharged to an x-ray tube after triggering the cathode electrode. The flash x-rays are then produced. The x-ray tube is of a demountable triode that is connected to a turbo molecular pump with a pressure of approximately 1mPa. As electron flows from the cathode electrode are roughly converged to a rod copper target of 3.0 mm in diameter by electric field in the x-ray tube, the weakly ionized linear plasma, which consists of copper ions and electrons, forms by target evaporating. At a charging voltage of 50 kV, the maximum tube voltage was almost equal to the charging voltage of the main condenser, and the peak current was about 20 kA. When the charging voltage was increased, the linear plasma formed, and the K-series characteristic x-ray intensities increased. The x-ray pulse widths were about 800 ns, and the time-integrated x-ray intensity had a value of about 30 μC/kg at 1.0 m from x-ray source with a charging voltage of 50 kV. The plasma x-rays were diffused after passing through two lead slits.

1. INTRODUCTION

Flash x-rays are high-dose-rate x-rays with short durations and are useful in order to perform high-speed radiography, and the maximum accelerating voltage has been increased to megavolt level using a Marx type high-voltage pulse generator[1] and an induction linear accelerator[2,3] to produce hard x-rays for military applications. Next, we have developed several different soft generators[4-8] to obtain soft

[a] Department of Physics, Iwate Medical University, 3-16-1 Honchodori, Morioka 020-0015, Japan
[b] Electrical Engineering, Hachinohe National College of Technology, 16-1 Tamonoki Uwanotai, Hachinohe 039-1104, Japan
[c] ITP, FHTW FB1 and TU-Berlin, Blankenhainer Str. 9, D 12249 Berlin, Germany
[d] Department of Physiology, School of Medicine, Tokai University, Boseidai, Isehara 259-1193, Japan
[e] Department of Cardiac Physiology, National Cardiovascular Center Research Institute, 5-7-1 Fujishirodai, Suita, Osaka 565-8565 Japan
[f] Department of Radiological Technology, College of Medical Science, Tohoku University, 1-1 Seiryocho, Sendai 980-0872, Japan
[g] Department of Radiological Technology, School of Health Sciences, Hirosaki University, 66-1 Honcho, Hirosaki 036-8564, Japan
[h] Shock Wave Research Center, Institute of Fluid Science, Tohoku University, 2-1-1 Katahira, Sendai 980-8577, Japan

radiograms, and repetitive generators[9-12] including stroboscopic generators[13-16] have been employed to perform multiple-shot and cine radiographies.

It is well known that a synchrotron generates high-dose-rate monochromatic x-rays using silicon single crystals, these rays play important roles in parallel radiography that is employed to perform high-resolution angiography and phase contrast imaging. However, because there are many important studies using a synchrotron, it is very difficult to obtain sufficient machine times for further applications. Recently, soft x-ray lasers[17,18] have been produced using a gas-discharge capillary, and the laser intensity increases with increases in the capillary length. However, it is not easy to increase the photon energy up to about 10 keV or higher using light amplification by stimulated emission. Without considering coherence, we have developed several different plasma flash x-ray generators[19-23] to increase K-series characteristic x-rays by forming weakly ionized linear plasma. In conjunction with the angle dependence of the bremsstrahlung x-rays, because the bremsstrahlung x-rays are absorbed and are converted into fluorescent x-rays, higher-intensity characteristic x-rays are produced from the plasma axial direction.

In the present work, we introduce a new plasma flash x-ray generator for generating intense and sharp characteristic x-rays such as x-ray laser, and we have measured radiographic characteristics of weakly ionized linear plasma of copper.

2. GENERATOR

2.1. High-Voltage Circuit

Figure 1 shows block diagram of a high-intensity plasma flash x-ray generator. This generator consists of the following essential components: a high-voltage power supply, a high-voltage condenser with a capacity of about 200 nF, a turbo-molecular pump, a krytron pulse generator as a trigger device, and a flash x-ray tube. In this generator, a low-impedance transmission line is employed in order to increase maximum tube current. The high-voltage main condenser is charged up to 50 kV by the power supply, and electric charges in the condenser are discharged to the tube after triggering the cathode electrode by the trigger device. The plasma flash x-rays are then produced.

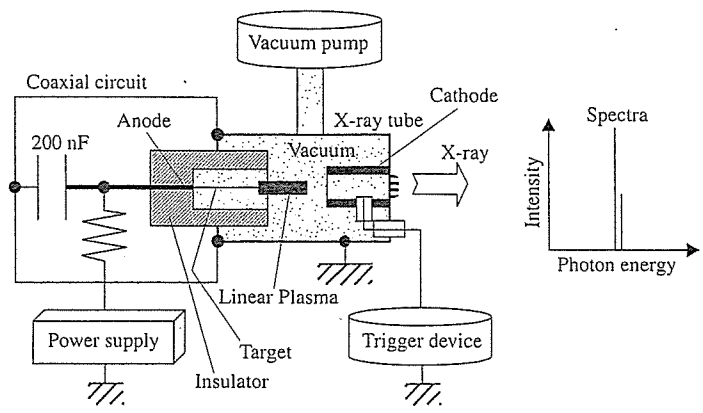

Fig. 1: Block diagram of the high-intensity plasma flash x-ray generator.

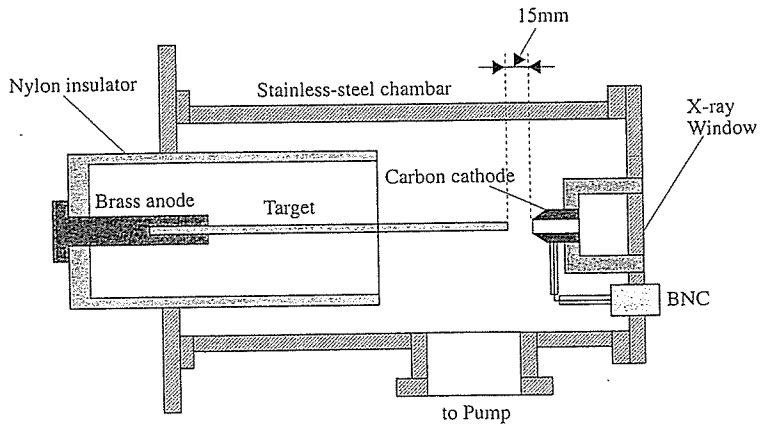

Fig. 2: Schematic drawing of the flash x-ray tube with a rod target.

2.2. X-ray Tube

The x-ray tube is of a demountable cold-cathode triode that is connected to the turbo molecular pump with a pressure of approximately 1 mPa (Fig. 2). This tube consists of the following major parts: a pipe-shaped carbon cathode with a bore diameter of 10.0 mm, a trigger electrode made from a copper wire, a stainless-steel vacuum chamber, a nylon insulator, a polyethylene terephthalate (Mylar) x-ray window of 0.25 mm, and a rod-shaped copper target of 3.0 mm in diameter.

The distance between the anode and cathode electrodes is approximately 15 mm, and the trigger electrode is set in the cathode electrode. As electron beams from the cathode electrode are roughly converged to the target by electric field in the tube, the weakly ionized linear plasma, which consists of copper ions and electrons, forms around the fine target by evaporating.

2.3. Principle of Characteristic X-ray Irradiation

If we assume that the thickness of linear plasma has a small value, x-ray spectra from the transverse direction is almost equivalent to standard distribution from a conventional x-ray generator having a hot-cathode tube. In the plasma, bremsstrahlung spectra with photon energies of higher than K-absorption edge are effectively absorbed and are converted into fluorescent x-rays. Next, the plasma transmits the fluorescent rays easily, and bremsstrahlung rays with energies of lower than K-edge are also absorbed by the plasma. In addition, because K-fluorescent yield corresponding to conversion efficiency approaches one according to increases in atomic number, intense characteristic x-rays are generated from the plasma-axial direction (Fig. 3).

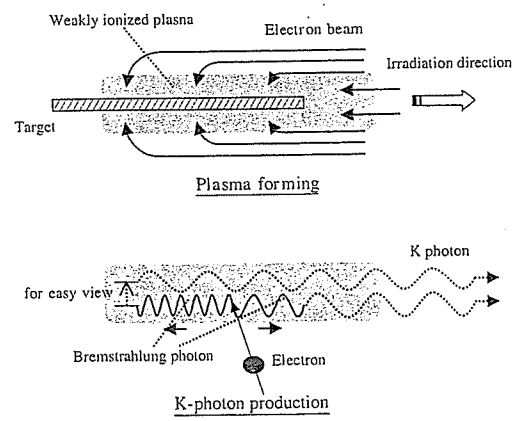

Fig. 3: Principle for generating intense and sharp characteristic x-rays.

3. CHARACTERISTICS

3.1. Tube Voltage and Current

Tube voltage and current were measured by a high-voltage divider with an input impedance of 1 GΩ and a current transformer, respectively. Figure 4 shows time relation between the tube voltage and current. At the indicated charging voltage, they roughly displayed damped oscillations. When the charging voltage was increased, both the maximum tube voltage and current increased. At a charging voltage of 50 kV, the maximum tube voltage was almost equal to the charging voltage of the main condenser, and the maximum tube current was about 20 kA.

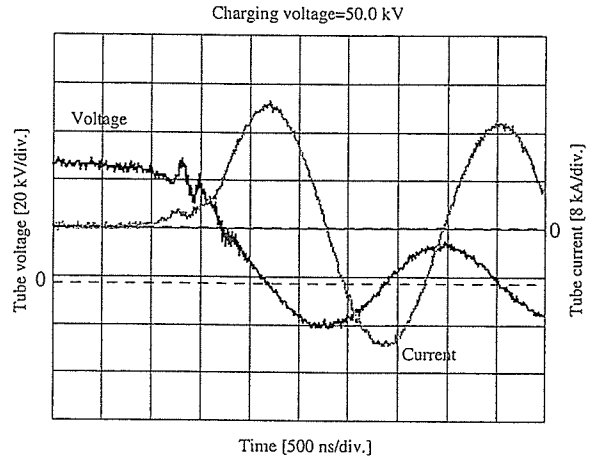

Fig. 4: Tube voltages and currents with a charging voltage of 50.0 kV.

3.2. X-ray Output

X-ray output pulse was detected using a combination of a plastic scintillator and a photomultiplier (Fig. 5). The x-ray pulse height substantially increased with corresponding increases in the charging voltage. The x-ray pulse widths were about 800 ns, and the time-integrated x-ray intensity measured by a thermoluminescence dosimeter (Kyokko TLD Reader 1500 having MSO-S elements without energy compensation) had a value of about 30 μC/kg at 1.0 m from the x-ray source with a charging voltage of 50 kV.

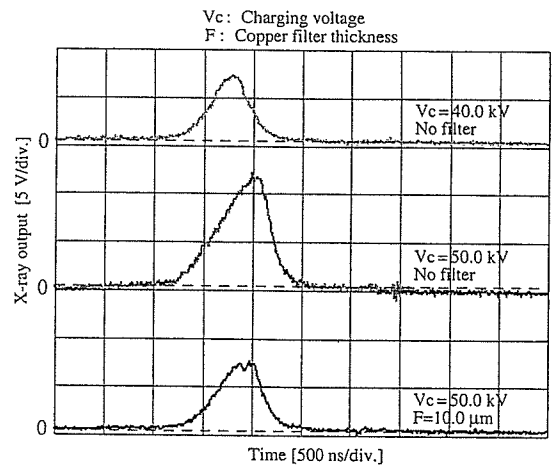

Fig. 5: X-ray outputs at the indicated charging voltages.

3.3. X-ray Source

In order to measure images of the plasma x-ray source, we employed a pinhole camera with a hole diameter of 100 μm (Fig. 6). When the charging voltage was increased, the plasma x-ray source grew, and both the spot dimension and intensity increased.

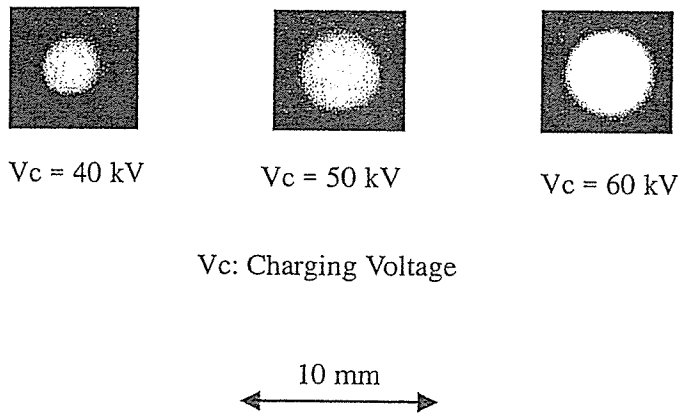

Fig. 6: Images of the plasma x-ray source.

3.4. X-ray Spectra

X-ray spectra from the plasma source were measured by a transmission-type spectrometer with a lithium fluoride curved crystal of 0.5 mm in thickness (Fig. 7). The spectra were taken by a computed radiography (CR) system[24] having a wide dynamic range, and relative x-ray intensity was calculated from Dicom digital data. Figure 8 shows measured spectra from the copper target. In fact, we observed quite intense-sharp lines of K-series characteristic x-rays such as lasers and hardly detected bremsstrahlung rays. The characteristic x-ray intensity substantially increased with corresponding increases in the charging voltage.

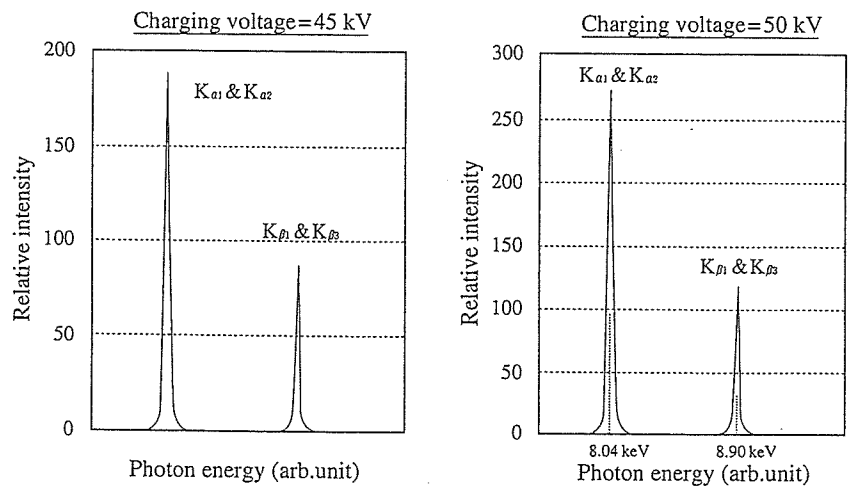

Fig. 7: X-ray spectra from the copper-plasma target at the indicated conditions.

3.5. X-ray Diffraction by Slits

Although coherence is the most important factor in x-ray amplification, it is quite difficult to measure the coherence, because the x-rays for biomedical radiography can penetrate various objects easily. For this research, in order to measure difference of characteristics between the incoherent and plasma x-rays, we employed two lead slits in order to measure the diffraction power of characteristic x-rays. As compared with incoherent x-rays from a hot-cathode x-ray tube, the characteristic x-rays from the linear plasma are diffracted and diffused greatly after passing through two slits.

4. RADIOGRAPHY

The plasma radiography was performed by the CR system, and the condenser charging voltage and the distance between the x-ray source and imaging plate were 50 kV and 1.2 m, respectively.

An enlarged radiogram of a test chart for measuring image resolution is shown in Fig. 8. The image resolution is determined by the focal spot dimension, the distance between the x-ray source and imaging plate, and the distance between the radiographic object and imaging plate. In the CR radiography, the resolution had a value of about 100 μm, and the resolution was almost equal to the CR resolution. Figure 9 shows radiograms of a concentric-circled steps of 5.0 mm made of polymethyl methacrylate (PMMA) with a maximum height of 25.0 mm. In this radiography, we obtained almost the same contrast images even when the monochromatic filter was employed or not. A radiogram of a vertebra is shown in Fig. 10, and the fine structures of the bone are observed vividly. Figure 11 shows an angiogram of a heart extracted from a rabbit using iodine-based microspheres of 20 μm. Although the characteristic x-rays hardly penetrated the heart, fine blood vessels were comparatively visible.

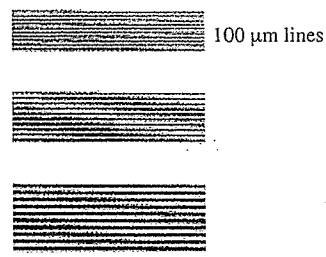

Fig. 8: Enlarged radiogram of a test chart.

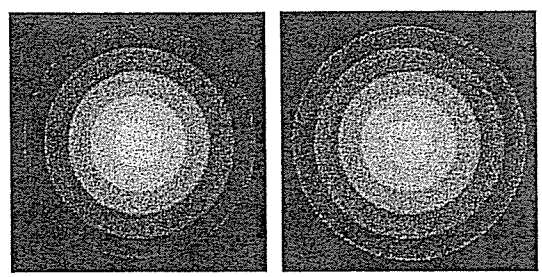

Fig. 9: Radiograms of a concentric-circled steps of 5.0 mm made of polymethyl methacrylate (PMMA) with a maximum height of 25.0 mm at the indicated conditions.

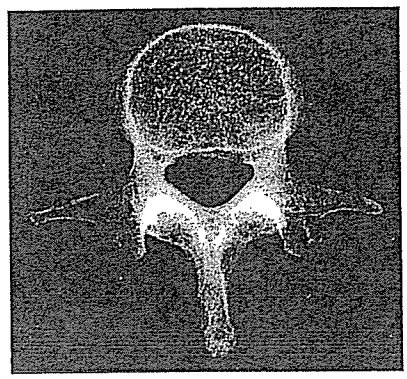

Fig. 10: Radiogram of a vertebra.

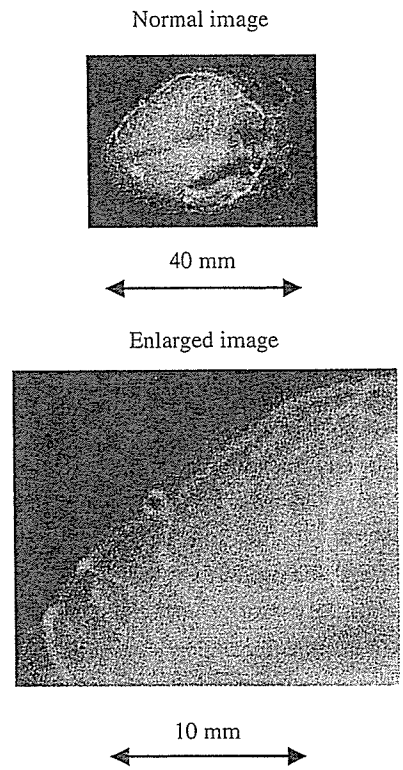

Fig. 11: Angiogram of a heart extracted from a rabbit.

5. DISCUSSION

For this research, we have obtained intense and sharp K-series characteristic x-rays such as laser, and have performed quite soft quasi-monochromatic radiography. Because it is quite difficult to generate higher-dose-rate x-rays in a lower photon energy region of about 10 keV or lower using a conventional x-ray generator having a hot-cathode tube, it goes without saying that plasma flash x-ray generator has the strong power to produce intense and high-dose-rate characteristic x-rays without bremsstrahlung rays. In this generator, the x-rays are produced from both solid and plasma targets, and the solid target is covered with a plasma cloud. In order to simplify the consideration, if we assume that the solid target is negligible, the K photons are produced from the weakly ionized linear plasma by the fine target evaporation. In the plasma target, although both the bremsstrahlung and characteristic x-rays are generated, bremsstrahlung x-rays generated in the plasma are absorbed and converted into fluorescent x-rays. Thus the absorbed bremsstrahlung x-ray intensity I_{ab} and the converted fluorescent x-ray intensity I_{kc} are roughly given by:

$$I_{ab} = K_1 \int_0^a \int_{E_k}^{\infty} I(E)[1-\exp\{-\mu_p(E) \cdot x\}]dE \quad dx, \tag{1}$$

$$I_{kc} = K_2 \cdot \omega_k \cdot I_{ab} = \sum_{i=1}^{n} I_k(E_i). \tag{2}$$

Here, E_k is the critical excitation energy of K-series characteristic x-rays, $I(E)$ is the bremsstrahlung x-ray distribution as a function of photon energy E, $\mu_p(E)$ is the linear absorption coefficient of plasma, $I_k(E_i)$ is the converted i th K-series characteristic x-ray intensity, E_i is the photon energy of characteristic x-rays, ω_k is the K-fluorescent yield, a is the plasma length, x is the plasma depth, n is the number of characteristic x-rays, and K_1 and K_2 are constants. In this case, the total characteristic x-ray intensity I_k from the plasma is written as:

$$I_k = (na)^{-1} \sum_{i=1}^{n} \{I_k(E_i) + I'_k(E_i)\} \int_0^a \exp\{-\mu_p(E_i) \cdot x\}\, dx, \tag{3}$$

where $I'_k(E_i)$ is the initial K-series x-ray intensity generated in the plasma.

Using this plasma x-ray generator, since we hardly observe difference between $K_{\alpha 1}$ and $K_{\alpha 2}$ lines and can obtain only K_α lines by absorbing K_β lines using a monochromatic filter, these intense characteristic x-rays without bremsstrahlung rays may be applied to perform quasi-monochromatic or monochromatic high-speed radiography instead of the synchrotron.

ACKOWLEDGEMENTS

This work was supported by Grants-in-Aid for Scientific Research (12670902, 13470154 and 13877114) from MECSST, Test of Fostering Potential of Japan Science and Technology Corporation, New Energy and Industrial Technology Development Organization, and Cardiovascular Disease (H13C-1) from MHLW.

REFERENCES

1. R. Germer, "X-ray flash techniques," *J. Phys. E: Sci. Instrum.*, **12**, pp. 336-350, 1979.
2. C. Cavailler, "AIRIX: an induction accelerator facility developed at CEA for flash radiography in detonics," *SPIE*, **3516**, pp. 25-35, 1998.
3. C. Cavailler, "AIRIX- a new tool for flash radiography in detonics," *SPIE*, **4183**, pp. 23-35, 2000.
4. E. Sato, H. Isobe and F. Hoshino, "High intensity flash x-ray apparatus for biomedical radiography," *Rev. Sci. Instrum.*, **57**, pp. 1399-1408, 1986.
5. E. Sato, S. Kimura, S. Kawasaki, H. Isobe, K. Takahashi, Y. Tamakawa and T. Yanagisawa, "Repetitive flash x-ray generator utilizing a simple diode with a new type of energy-selective function," *Rev. Sci. Instrum.*, **61**, pp. 2343-2348, 1990.
6. E. Sato, A. Shikoda, S. Kimura, M. Sagae, T. Oizumi, K. Takahashi, Y. Hayasi, T. Shoji, K. Shishido, Y. Tamakawa and T. Yanagisawa, "Repetitive compact flash x-ray generators for soft radiography," *SPIE*, **1801**, pp. 628-642, 1992.
7. E. Sato, M. Sagae, K. Takahashi, T. Oizumi, H. Ojima, K. Takayama, Y. Tamakawa, T. Yanagisawa, A. Fujiwara and K. Mitoya, "High-speed soft x-ray generators in biomedicine," *SPIE*, **2513**, pp. 649-667, 1994.
8. E. Sato, M. Sagae, K. Takahashi, A. Shikoda, T. Oizumi, H. Ojima, K. Takayama, Y. Tamakawa, T. Yanagisawa, A. Fujiwara and K. Mitoya, "Dual energy flash x-ray generator," *SPIE*, **2513**, pp. 723-735, 1994.
9. A. Shikoda, E. Sato, M. Sagae, T. Oizumi, Y. Tamakawa and T. Yanagisawa, "Repetitive flash x-ray

generator having a high-durability diode driven by a two-cable-type line pulser," *Rev. Sci. Instrum.*, **65**, pp. 850-856, 1994.

10. E. Sato, K. Takahashi, M. Sagae, S. Kimura, T. Oizumi, Y. Hayasi, Y. Tamakawa and T. Yanagisawa, "Sub-kilohertz flash x-ray generator utilizing a glass-enclosed cold-cathode triode," *Med. & Biol. Eng. & Comput.*, **32**, pp. 289-294, 1994.
11. K. Takahashi, E. Sato, M. Sagae, T. Oizumi, Y. Tamakawa and T. Yanagisawa, "Fundamental study on a long-duration flash x-ray generator with a surface-discharge triode," *Jpn. J. Appl. Phys.*, **33**, pp. 4146-4151, 1994.
12. E. Sato, M. Sagae, A. Shikoda, K. Takahashi, T. Oizumi, M. Yamamoto, A. Takabe, K. Sakamaki, Y. Hayasi, H. Ojima, K. Takayama and Y. Tamakawa, "High-speed soft x-ray techniques," *SPIE*, **2869**, pp. 937-955, 1996.
13. E. Sato, A. Shikoda, S. Kimura, M. Sagae, H. Isobe, Y. Tamakawa and T. Yanagisawa, "Kilohertz-range flash x-ray generator utilizing a triode in conjunction with an extremely hot cathode," *Rev. Sci. Instrum.*, **62**, pp. 2115-2120, 1991.
14. E. Sato, M. Sagae, K. Takahashi, A. Shikoda, T. Oizumi, Y. Hayasi, Y. Tamakawa and T. Yanagisawa, "10 kHz microsecond pulsed x-ray generator utilizing a hot-cathode triode with variable durations for biomedical radiography," *Med. & Biol. Eng. & Comput.*, **32**, pp. 295-301, 1994.
15. E. Sato, T. Ichimaru, H. Obara, M. Zuguchi, H. Mori, E. Tanaka, T. Usuki, K. Sato, H. Ojima, K. Takayama, K. Sakamaki and Y. Tamakawa, "Condenser-discharge stroboscopic x-ray generator for medical radiography," *SPIE*, **4183**, pp. 383-393, 2000.
16. E. Sato, Y. Hayasi and Y. Tamakawa, "Recent stroboscopic x-ray generators and their applications to high-speed radiography," *Ann. Rep. Iwate Med. Univ. Lib. Arts & Sci.*, **35**, pp. 1-11, 2000.
17. J.J.G. Rocca, J.L.A. Chilla, S. Sakadzic, A. Rahman, J. Filevich, E. Jankowska, E.C. Hammarsten, B.M. Luther, H.C. Kapteyn, M. Murnane and V.N. Shlyapsev, "Advances in capillary discharge soft x-ray laser research," *SPIE*, **4505**, pp. 1-6, 2001.
18. S. Le Pape, Ph. Zeitoun, J.J.G. Rocca, A. Carillon, P. Dhez, M. Francois, S. Hubert, M. Idir and D. Ros, "Characterisation of an x-ray laser beam," *SPIE*, **4505**, pp. 23-34, 2001.
19. E. Sato, Y. Suzuki, Y. Hayasi, E. Tanaka, H. Mori, T. Kawai, K. Takayama, H. Ido and Y. Tamakawa, "High-intensity quasi-monochromatic x-ray irradiation from the linear plasma target," *SPIE*, **4505**, pp. 154-164, 2001.
20. E. Sato, Y. Hayasi, E. Tanaka, H. Mori, T. Kawai, H. Obara, T. Ichimaru, K. Takayama, H. Ido, T. Usuki, K. Sato and Y. Tamakawa, "Polycapillary radiography using a quasi-x-ray laser generator," *SPIE*, **4508**, pp. 176-187, 2001.
21. E. Sato, Y. Hayasi, E. Tanaka, H. Mori, T. Kawai, T. Usuki, K. Sato, H. Obara, T. Ichimaru, K. Takayama, H. Ido and Y. Tamakawa, "Quasi-monochromatic radiography using a high-intensity quasi-x-ray laser generator," *SPIE*, **4682**, pp. 538-548 2002.
22. E. Sato, Y. Hayasi, T. Usuki, K. Sato, K. Takayama and H. Ido, "Characteristics of a capillary-discharge flash x-ray generator" *SPIE*, **4786**, pp. 173-182, 2002.
23. E. Sato, Y. Hayasi, E. Tanaka, H. Mori, T. Kawai, K. Takayama and H. Ido, "Irradiation of intense characteristic x-rays from weakly ionized linear plasma," *Proc 3rd Korea-Japan Joint Meeting on Medical Physics*, Gyeongju, pp. 396-399, 2002.